Experimental and theoretical study on bond behavior of GFRP bars in steel fiber reinforced self compacting concrete

H. Mazaheripour & J. O. A. Barros
ISISE, University of Minho, Guimaraes, Portugal

M. Pepe & A. Giliberti & E. Martinelli
University of Salerno, Fisciano, Italy

ABSTRACT: To estimate the cracking and the deformational behavior of steel fiber reinforced self-compacting concrete (SFRSCC) beams reinforced with glass fiber reinforced polymer (GFRP) bars, it is fundamental to understand the interfacial bond behavior of embedded bars. Hence, the evaluation of the bond behavior between GFRP and (SFRSCC) was investigated in this study. A closed-form formulation was derived, adopting a new local bond stress-slip relationship. Furthermore, an experimental program composed of pullout bending tests was carried out in order to assess the influence of the following parameters on the bond behavior: bar diameter, bar surface treatment, embedment length and SFRSCC cover thickness. Finally, a numerical simulation was performed with a FEM-based computer program in order to simulate the bond behavior between GFRP bar and SFRSCC by means of a non-linear bond-slip relationship assigned to the interface finite element. The predictive performance of the theoretical models was appraised by comparing experimental and numerical results.

1 INSTRUCTIONS

Due to the lower young's modulus of Glass FRP (GFRP) bar, serviceability requirements such as crack width and crack spacing become main concerns in GFRP reinforced concrete elements. To predict the cracking behavior of GFRP RC beams, a bond-slip constitutive law is required for modeling the bond between longitudinal GFRP bars and surrounding concrete. Some experimental and theoretical investigations have been carried out in this area in the last two decades (Achillides & Pilakoutas 2004, Aiello et al. 2007, Davalos et al. 2008, Baena et al. 2009 and Robert et al. 2010); However, the lack of agreement is found in the literature due to the diversity of techniques for surface treatment of the GFRP bars, since this has a strong impact on its interfacial bond behavior (Okelo et al. 2005, Lee et al. 2008). Furthermore, the bond behavior is also very susceptible to the influence of other various parameters.

The presence of steel fiber reinforced self-compacting concrete (SFRSCC), which in the ambit of the present research project has the purpose of replacing the steel stirrups, gives further justification for this experimental, analytical and numerical studies.

Some analytical bond-slip laws were developed, namely: Bertero-Eligehausen-Popov (BEP) model (Eligehausen et al. 1983), Cosenza-Manfredi-Realfonzo (CMR) model (Cosenza et al. 1997) and a modified BEP model by Focacci et al. 2000. In all these methods, the unknown parameters related to the bond-slip constitutive law are determined by using experimental results that, in general, are obtained from direct pullout tests.

In this paper, a 4-linear bond-slip diagram is proposed, and closed-from equations were derived by solving the non-linear differential equation governing the debonding process (Russo et al. 1990). Furthermore, an extensive experimental program composed of pullout bending tests, based on a test setup similar to that recommended by RILEM, was carried out, and relevant results are presented in this paper. The comprehensive analysis of all experimental results is available elsewhere (Pepe 2011).

Finally, a finite element model was implemented by using an interface finite element with non-linear behavior to simulate the bond behavior between GFRP bar and SFRSCC. The performance of the model is appraised by considering the obtained experimental results.

2 ANALYTICAL BOND MODEL

An analytical model to simulate the bond behavior between GFRP bars and fiber reinforced concrete is presented hereafter.

2.1 *Governing equation*

The differential equation that governs the bond behavior along the embedment length of a bar can be written as follow (Focacci et al. 2000):

$$\frac{d^2 d}{dx^2} - J_1\, t\,(d\,(x)) = 0 \tag{1}$$

where J_1 is the ratio between the perimeter (πd_b) and axial stiffness ($E_b A_b$) of the bar, being, d_b, E_b and A_b the diameter, the modulus of elasticity and the cross-sectional area of the bar, respectively. In equation (1) δ is the punctual relative displacement between the GFRP and SFRSCC. Based on the equilibrium equation along the bar, the following equations can be also deduced:

$$s_b\,(x) = E_b \frac{dd}{dx} \tag{2}$$

and

$$t\,(x) = \frac{1}{J_1}\frac{d^2 d}{dx^2} \tag{3}$$

where σ_b is the normal stress in the bar and τ is the bond shear stress along the bond length.

The above equations were derived by assuming a linear and elastic behavior for the embedded bar and considering null deformability for the surrounding SFRSCC.

2.2 *Local bond-slip relationship*

To solve equation (1), the local bond-slip relationship, τ-δ, shown in Figure 1 and formulated in equation (4) is proposed. This diagram simulates four different phases of the bond process. After the rigid branch (0-τ_0), which represents the overall initial shear strength of the joint, the first debonding phase is simulated by an elastic ascending branch up to the bond strength (τ_1) that occurred at a slip of δ_1. By simplification, it is assumed that the bond damage accumulated during this phase is reflected in the second phase, herein designated as plastic phase, where the bond strength is maintained between δ_1 and δ_2. By increasing the slip, the bond stress decreases due to the increase of damage in the bond mechanisms along the embedment length during this softening phase that ends at δ_3. For slips higher than δ_3 it is assumed that the friction between bar and concrete provides a constant residual bond strength (τ_3) for the embedded bar. This can be proved by earlier work carried out by Baena et al. and Hao et al. 2009).

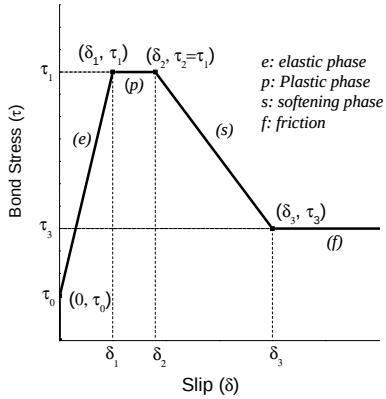

Figure 1. Local bond-slip relationship.

$$t\,(d) = \begin{cases} t_0 + \dfrac{t_1 - t_0}{d_1} d & 0 \le d < d_1 \\ t_1 = t_2 & d_1 \le d < d_2 \\ t_2 - \dfrac{t_2 - t_3}{d_3 - d_2}(d - d_2) & d_2 \le d < d_3 \\ t_3 & d \ge d_3 \end{cases} \tag{4}$$

2.3 *Theoretical pullout force*

By substituting the equation (4) in equation (1), the derived non-linear differential equation can be solved for the different proposed phases by introducing the boundary conditions of an infinite bond length. The closed-form equations are similar to the formulation derived by Bianco et al 2009 in case of NSM CFRP strips. In fact, to adjust this formulation for the case of a GFRP bar, softening and free slipping phases of this model were replaced by the plastic (*p*) and friction (*f*) phases, respectively.

For each phase indicated in Figure 1, the corresponding force transferred to concrete $V(\delta_i(x))$, can be determined from the following equation:

$$V(d_i) = \begin{cases} p\, d_b \int_0^{L_{tr}^e (d_i)} t^e (x^e)\, dx^e & 0 \le d_i \le d_1 \\ V^e(d_1) + p\, d_b \int_0^{L_{tr}^p (d_i)} t^p (x^p)\, dx^p & d_1 < d_i \le d_2 \\ V^e(d_1) + V^p(d_2) + p\, d_b \int_0^{L_{tr}^s (d_i)} t^s (x^s)\, dx^s & d_2 < d_i \le d_3 \\ V^e(d_1) + V^p(d_2) + V^s(d_3) + p\, d_b \int_0^{L_{tr}^f (d_i)} t^f (x^f)\, dx^f & d_3 < d_i \end{cases} \tag{5}$$

where the superscript letters represent the phases shown in Figure 1. The transfer bond length of whatever value of imposed slip, $L_{tr}(\delta_i(x))$, included in equation (5), can be calculated by using the following equilibrium equation along the bar:

$$V\big(d_i(x)\big) = E_b A_b \frac{dd_i(x)}{dx} \big(L_{tr}^j (d_i(x))\big), \quad (j = e, p, s, f) \tag{6}$$

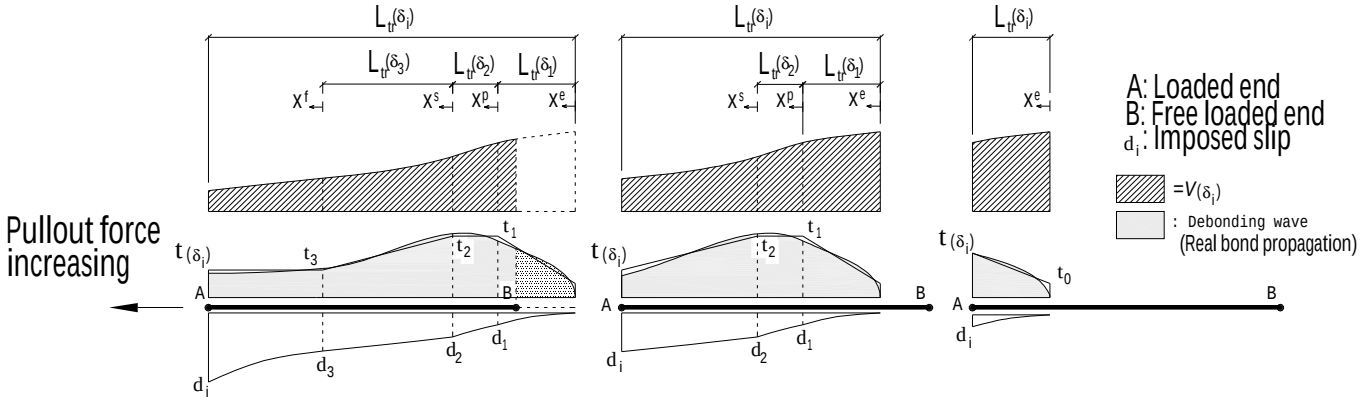

Figure 2. Debonding progress for finite bond length.

The right side of equation (6) is the pullout force in the bar that needs to be balanced with $V(\delta_i(x))$. Substituting (5) in (6), this last equation can be solved in order to provide the L_{tr}corresponding to the value of imposed slip δ_i.

By solving the integrals in (5), the theoretical pullout force can be determined for each value of imposed end slip ($\delta_i(x)$).

To extend the formulation for the case of a finite embedment length (L_R), the debonding progress is known as a "progressive wave" that moves along the bond length (Bianco et al. 2009). When the debonding process reaches the free extremity of the bond length, the bar at this point (point B in Figure 2) starts to slip with the lower rate of increment comparing with the imposed slip. By increasing the pullout force, the slip rate at free loaded end (δ_{Fi}) also increases. When δ_{Fi} exceeds δ_3 (obviously $\delta_i > \delta_3$), a constant residual bond stress is assumed along the embedment length (L_R) and, consequently, a constant residual pullout force is attained. This progress is schematically illustrated in Figure 2, where $L_{tr}(\delta_1)$, $L_{tr}(\delta_2)$ and $L_{tr}(\delta_3)$ represent the maximum invariant value of transfer length that can undergo elastic, plastic and friction phase, respectively.

To calculate the theoretical pullout force in case of a finite bond length, the possible configurations between L_R and L_{tr} should be taken into account for whatever value of imposed slip. For instance, in elastic phase ($0 < \delta_i \leq \delta_1$), as first branch, two possible configurations can be taken place between L_R and $L_{tr}(\delta_1)$; $L_R > L_{tr}(\delta_1)$:

$$V^e(d_i) = p\, d_b \int_0^{L^e_{tr}(d_i)} t^e(x^e)\, dx^e \tag{7}$$

and the corresponding value at free end, δ_F, is equal to zero.

or $L_R \leq L_{tr}(\delta_1)$

$$V^e(d_i) = p\, d_b \int_{L^e_{tr}(d_i) - L_R}^{L^e_{tr}(d_i)} t^e(x^e)\, dx^e \tag{8}$$

and free end slip (δ_{fi}) is:

$$d_{Fi}(d_i) = d^e(L^e_{tr}(d_i) - L_R) \tag{9}$$

The same equations can be stated for other phases based on the possible configurations between L_R and L_{tr}.

For each value of imposed slip δ_i, the corresponding force transferred to concrete $V(\delta_i)$, the transfer bond length $L_{tr}(\delta_i)$ and the slip at free loaded end δ_{Fi} can be calculated. Therefore, the theoretical pullout force versus slip at loaded and free ends can be obtained by means of the proposed bond model.

3 EXPERIMENTAL PROGRAM

To evaluate the interfacial bond behavior between GFRP bar and SFRSCC, an experimental program composed of pullout bending tests, based on a test setup similar to the one recommended by RILEM 1982, was carried out (Pepe 2011). In this section, a brief description of the experimental program is done and the main results are presented.

3.1 *Test program*

A total of 36 pullout beam bending tests were executed to assess the influence of following parameters on the bond behavior: bar diameters (ϕ8 and ϕ12), bond length, SFRSCC cover thickness, and surface of GFRP bars. For this purpose, three different bond lengths (l_e=5ϕ, 10ϕ and 20ϕ), two different surfaces of GFRP bar (ribbed and sand-coated), two nominal bar diameters of 8 and 12 mm (only for ribbed bar) and two SFRSCC cover thicknesses (15 and 30 mm) were considered.
Figure 3 shows the test setup and the adopted monitoring system. For each specimen, the slip at both loaded and free ends were measured, as well as the pullout force in the bar. The slip was recorded by using two Linear Voltage Differential Transducers (LVDT), and the pullout force was calculated by multiplying the strain measured in the strain gauge by the elasticity modulus and the bar cross sectional area. Two slipping test control regimes of different

slip rate were adopted: 3 μm/sec until 5 mm slip; 5 μm/sec up to the end of the test.

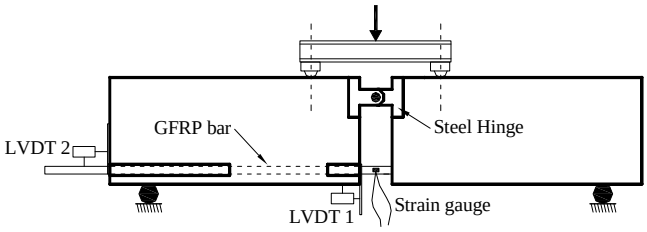

Figure 3. Pullout bending test setup.

3.2 *Materials*

Two blocks of each specimen is made by SFRSCC from a mix composition of ordinary Portland cement CEM I 42.5 R (412 kg/m^3), limestone filler (353 kg/m^3), fine and coarse river sand (179 and 655 kg/m^3, respectively), crushed granite gravel aggregate (588 kg/m^3) with maximum size of 12 mm, 1.9% of cement content of super-plasticizer, an water/cement ratio of 0.39, and 60 kg/m^3 hooked ends steel fibers with a length (L_f) and a diameter (d_f) of 33 mm and 0.55 mm, respectively (L_f/d_f=60).

The compressive strength, the Young's modulus and the flexural strength of the used SFRSCC was, respectively, 63.68 MPa (CoV=5.51%), 30.36 GPa (CoV=15.48%) and 6.28 MPa (17.48%). Figure 4a shows the tensile stress-strain diagram obtained by applying the inverse analysis (Cunha 2007) to the force-crack mouth opening displacement (CMOD) relationships determined experimentally. More details about characterization of the developed SFRSCC can be found elsewhere (Mazaheripour et al. 2012).

As mentioned above, two types of GFRP bars in terms of surface treatments were selected for the experimental program. The first, which is called "deformed" bar hereafter, is a kind of ribbed bar with the rib height of 4-6% and 3-5% of bar diameter for nominal 12 and 8 mm bars, respectively. The rib spacing is 8.5 mm for both bars. The second type is a sand-coated bar, which is assumed as "smooth" bar in this study. Spherical natural quartz-crystal sand with triangular structure was used for sand-coating. Both bars are being produced by two European Companies. Figure 4b shows the tensile stress-strain relationship, as well as the value of elasticity modulus for the two types of GFRP bars. According to the supplier, the ultimate tensile strength for the deformed bars of 8 and 12 mm diameter is 1500 and 1350 MPa, respectively, and 1000 MPa for the smooth bar.

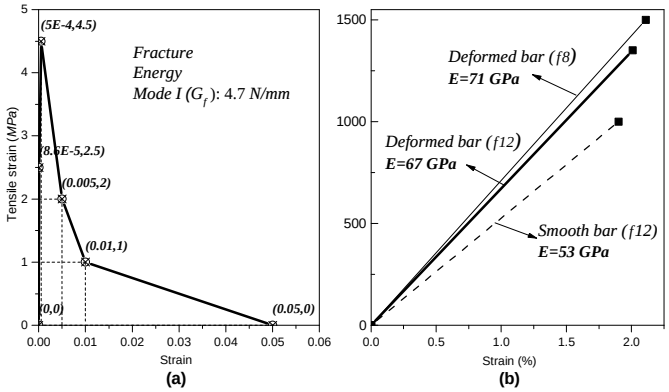

Figure 4. Tensile stress-strain relationship: (a) SFRSCC; (b) GFRP bars.

3.3 *Experimental outline*

The relationships between the pullout force and the slip at loaded and free ends were obtained for all the specimens. The pullout failure was observed for all specimens with the exception of one specimen reinforced with 8 mm bar diameter and 20ϕ bond length. Four tests were incomplete due to the shear failure of SFRSCC. The shear strengthening technique (by using carbon fiber reinforced polymer) proposed by Dias & Barros 2011 was utilized to avoid this failure in the remaining specimens, but without interfering with the bond conditions of the GFRP bar.

Table 1. Average values of the experimental results.

l_e	s_{lm}		s_{fm}		$\bar{F}_{lm}$		$\bar{t}_m$ ***	
	C_{15} *	C_{30} **	C_{15}	C_{30}	C_{15}	C_{30}	C_{15}	C_{30}
Deformed bar - 8 mm bar diameter								
5ϕ	0.33	0.34	0.24	0.27	20.38	19.96	20.28	19.86
10ϕ	0.89	0.75	0.15	0.32	30.88	35.32	14.45	16.70
20ϕ	1.57	2.22	0.12	0.29	57.14	66.77	13.50	15.78
Deformed bar - 12 mm bar diameter								
5ϕ	0.33	0.29	0.25	0.23	44.76	57.50	19.40	24.92
10ϕ	0.84	1.34	0.16	0.28	70.62	89.54	14.53	18.42
20ϕ	2.56	3.00	0.11	0.16	121.81	146.23	12.52	15.04
Smooth bar - 12 mm bar diameter								
5ϕ	0.48	0.49	0.10	0.09	42.06	50.82	18.40	21.94
10ϕ	0.81	1.50	0.09	0.08	62.92	76.64	12.94	15.76
20ϕ	2.04	2.36	0.08	0.10	98.74	106.24	10.26	10.26

* Data related to specimens with 15 mm concrete cover thickness.
** Data related to specimens with 30 mm concrete cover thickness.
*** The value obtained by multiplying modification factor which normalized the impact of SFRSCC compressive strength for different concrete mix batches.

The mean loaded end slip (s_{lm}) and free end slip (s_{fm}) at the maximum average pullout force ($\bar{F}_{lm}$) are reported in Table 1. Furthermore, the maximum average bond strength ($\bar{t}_m$) is indicated in the last two columns. It should be noticed that $\bar{t}_m$ was obtained by assuming a constant bond stress distribution along the bond length. The highlighted values in the table belong to only a single test, due to the shear failure of the other specimens pertaining to these series.

In addition, the maximum bond stress for 12 mm bar diameter was almost equal or smaller to $\bar{t}_{max}$ of 8 mm bar diameter in case of 15 mm concrete cover; however, in the specimens with 30 mm concrete cover, a greater value of $\bar{t}_m$ was obtained with the

exception of the specimen with 20ϕ bond length. The difference is more pronounced in 5ϕ bond length and has the tendency to decrease with the increase of the bond length. It can be concluded that by increasing the bar diameter and the bond length the maximum pullout force becomes limited by the SFRSCC splitting strength, which is higher for thicker concrete cover.

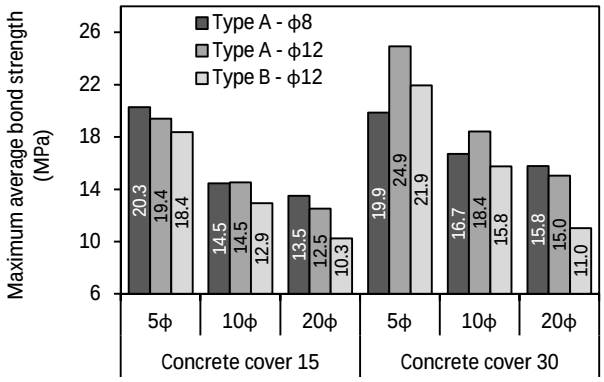

Figure 5. Comparison among the maximum average bond strength of GFRP bars in the pull bending test.

4 NUMERICAL INVESTIGATION

In this chapter some bond tests are numerically simulated by using the version 4.0 of FEMIX, a FEM-based computer program.

4.1 *Bond model*

To simulate the bond between GFRP bar and concrete, an interface finite element is used. The non-linear constitutive law assigned to the interface element is illustrated in Figure 6. The interface elements with an integration scheme of 2 points was applied with a constant normal stiffness of 0.1 MN/mm and a tangential stiffness provided by Equation (10) where the parameters were determined from inverse analysis, by fitting with the minimum error the pullout force versus loaded end slip curve (F-s_l) obtained from the experimental tests (the error is the ratio between the area limited by the experimental and the numerical F-s_l curves and the area underneath the experimental F-s_l curve).

$$t(d)=\begin{cases}\dfrac{t_0}{d_0}d & 0\le d<d_0\\ t_m\left(\dfrac{s}{s_m}\right)^{a_1} & d_0\le d<d_m\\ t_m\left(\dfrac{s}{s_m}\right)^{-a_2} & d_m\le d\end{cases} \quad (10)$$

4.2 *Material simulation*

4.2.1 *SFRSCC*

The smeared crack theory described by Barros et al. in 2011 was used to simulate the crack initiation and propagation in SFRSCC. The tri-linear diagram represented in Figure 4a was adopted to simulate the post-cracking tensile behavior of SFRSCC. Table 2 includes the values of the parameters of the smeared crack model.

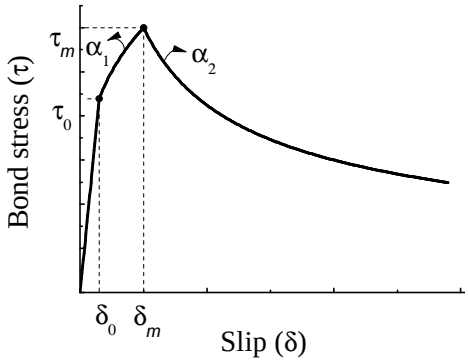

Figure 6. The bond-slip relationship assigned to the interface finite element bond model.

Table 2. Data of the smeared crack model adopted to simulate the material nonlinear behavior of SFRSCC.

Specifications	Values or descriptions
Type of element	2D Plane stress
Number of nodes	4 nodes
Integration scheme	2×2 Gauss Legendre
Young's modulus (E_c)	29 GPa
Poisson's ratio (v_c)	0.2
Energy fracture mode I	4.7 N/mm
Maximum tensile stress (f_{ct})	4.5 MPa
Threshold angle of new crack opening	30°
Shear behavior	(Barros et al. 2011)
Maximum number of crack per integration	2
Crack band width	The square root of the area of integration points

4.2.2 *GFRP bar*

To simulate GFRP bars, 2D Truss finite element of 2 nodes with 2 Gauss Legendre integration points with a linear stress-strain relationship up to failure was used (see figure 4b).

4.3 *Pullout bending test model*

A half-beam finite element model of pullout bending test is shown in Figure 7. The connection between interface finite elements, GFRP bar and SFRSCC is also illustrated in this figure.

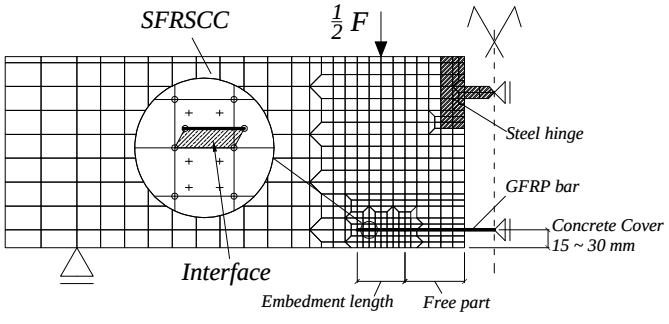

Figure 7. Finite element model of pullout bending test.

4.4 *Predictive performance of analytical and numerical models*

By selecting a set of parameters in Equation (4) and (10), the theoretical pullout force versus slip (at both loaded and free ends) can be obtained by the analytical (A) and numerical (N) approaches, respectively. The predictive performance of those models is assessed by comparing the obtained results with those recorded experimentally (Figure 8 and 9). The numerical and analytical results have been obtained by considering the minimum error with those experimental results in terms of pullout force versus loaded end slip.

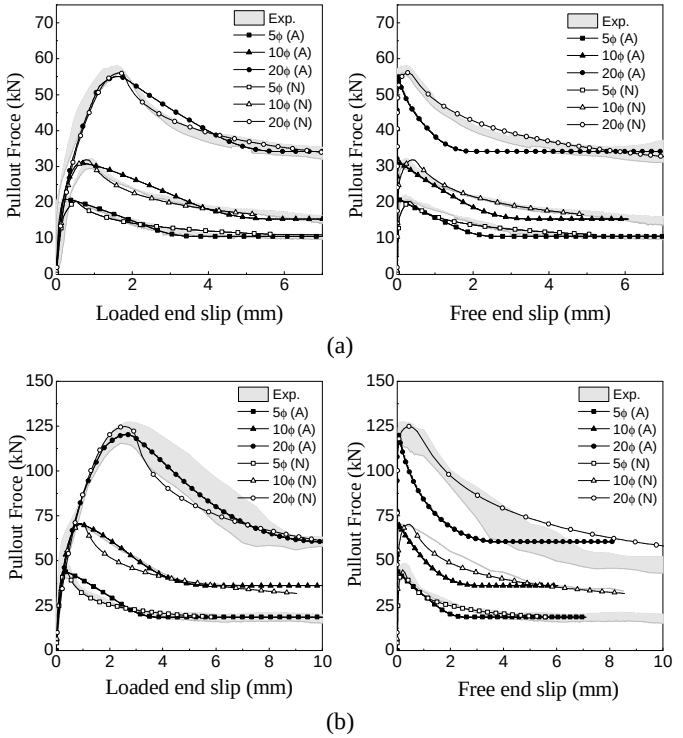

Figure 8. The comparison between experimental and analytical trends; (a) 8 mm bar diameter and (b) 12 mm bar diameter for deformed bar.

Figure 8 and 9 correspond to the specimens reinforced with deformed and smooth bars, respectively. As shown in these figures, by selecting a proper set of parameters for equations (4) and (10), a good agreement with the experimental results can be obtained, apart specimens reinforced with smooth bar and with a bond length of 20ϕ, where the matching is not satisfactory for both models. For these specimens, the abrupt load decay registered experimentally just after peak pullout force, was not well captured. After peak pullout load, the different bond behavior of deformed and smooth bar might be explained by the mechanical interlocking between bar and concrete that is pronounced for deformed bar (ribbed bar) and is null for smooth bar.

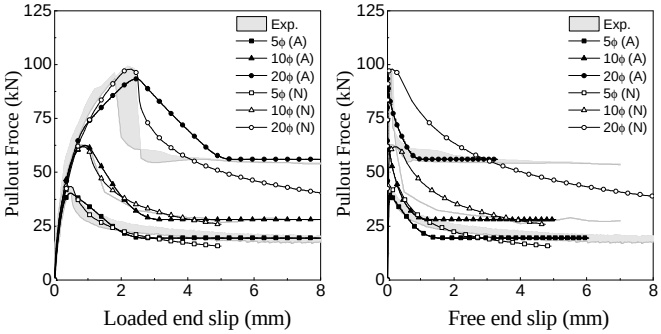

Figure 9. The comparison between experimental and theoretical trends; 12 mm bar diameter for Smooth bar.

In case of free slip (see right graphs in Figures 8 and 9), the numerical and analytical models show different performance in case of smooth and deformed bar. By comparing the experimental and numerical results at free end, the non-linear bond-slip law used for the interface finite element in FEMIX model shows an acceptable potential to predict the bond behavior of deformed bar for three applied bond lengths. This performance shows also an acceptable accuracy for smooth bar in case of 5ϕ bond length, however, the models was practically unable to simulate the bond behavior in case of higher bond length (10 and 20ϕ) due to abrupt decay in specimens after peak pullout load.

The values of the parameters obtained by inverse analysis from analytical model are summarized in Table 3 and 4 for the specimens with 15 mm and 30 mm SFRSCC cover thickness, respectively. However, the values adopted for the numerical simulations only correspond to the specimens with 15 mm concrete cover thickness.

Table 3. Values of bond parameters adopted by inverse analysis for specimens with 15 mm concrete cover (analytical approach).

l_e	δ_1 mm	δ_2 mm	δ_3 mm	τ_0 MPa	τ_1 MPa	τ_3 MPa	Err* %	τ_3/τ_1 %
Deformed bar - 8 mm bar diameter								
5ϕ	0.02	0.19	2.60	2.0	20.80	10.50	2.03%	50.4%
10ϕ	0.05	0.40	3.50	2.0	15.50	7.60	1.95%	49.0%
20ϕ	0.05	0.90	1.98	2.0	14.70	8.30	5.68%	56.46%
Deformed bar - 12 mm bar diameter								
5ϕ	0.01	0.17	2.60	3.0	19.50	8.20	3.25%	42.0%
10ϕ	0.04	0.33	3.00	3.0	16.10	8.00	0.14%	49.7%
20ϕ	0.08	0.60	3.80	3.0	14.80	6.70	2.20%	45.3%
Smooth bar – 12 mm bar diameter								
5ϕ	0.09	0.13	1.60	1.0	18.70	8.60	1.50%	46.0%
10ϕ	0.06	0.30	1.20	1.0	15.70	6.20	1.52%	39.5%
20ϕ	0.01	0.60	1.00	1.0	14.30	6.50	7.70%	45.4%

* Dividing the difference between area under the experimental and theoretical curve by experimental one.

4.5 *Maximum bond stress*

The maximum theoretical bond stress (τ_1) was obtained from the inverse analysis by fitting the experimental results with the minimum error. Figure 10 shows the relationship between the embedment length and τ_1. Similar to what happened with the

maximum average bond stress ($\bar{\tau}_m$) in section 4, the τ_1 has also decreased with the increase of L_e for both types of GFRP bars.

Table 4. Values for the bond parameters adopted in the inverse analysis for specimens with 30 mm concrete cover (analytical approach).

l_e	δ_1 mm	δ_2 mm	δ_3 mm	τ_0 MPa	τ_1 MPa	τ_3 MPa	Err* %	τ_3 / τ_1 %
Deformed bar - 8 mm bar diameter								
5ϕ	0.02	0.30	4.30	2.00	19.50	10.50	0.93%	53.8%
10ϕ	0.05	0.55	3.50	2.00	17.50	11.00	0.76%	62.8%
20ϕ	0.08	1.20	3.10	2.00	16.50	11.10	3.52%	67.3%
Deformed bar - 12 mm bar diameter								
5ϕ	0.02	0.30	1.30	3.0	24.80	16.50	1.39%	66.6%
10ϕ	0.10	1.05	2.80	3.0	19.50	10.40	1.18%	53.3%
20ϕ	0.10	2.00	4.30	3.0	17.20	6.60	2.40%	38.4%
Smooth bar – 12 mm bar diameter								
5ϕ	0.05	0.23	1.00	1.0	23.40	13.60	0.81%	58.1%
10ϕ	0.12	0.70	1.40	1.0	17.70	9.40	3.27%	53.1%
20ϕ	0.08	0.85	1.10	1.10	14.70	7.80	4.55%	53.1%

* Dividing the difference between area under the experimental and theoretical curve by experimental one.

Table 5. Values for the bond parameters adopted in the inverse analysis for specimens with 15 mm concrete cover (numerical model).

l_e	δ_0 mm	δ_m mm	α_1	α_2	τ_0 MPa	τ_m MPa	Err* %
Deformed bar - 8 mm bar diameter							
5ϕ	0.05	0.35	0.17	0.23	14.73	20.5	0.01%
10ϕ	0.05	0.45	0.17	0.30	11.36	16.5	0.01%
20ϕ	0.05	0.55	0.17	0.25	10.48	15.5	0.07%
Deformed bar - 12 mm bar diameter							
5ϕ	0.05	0.23	0.17	0.29	15.97	20.7	3.25 %
10ϕ	0.05	0.50	0.17	0.30	11.15	16.5	5.86%
20ϕ	0.05	1.00	0.15	0.40	10.08	15.8	3.90%
Smooth bar - 12 mm bar diameter							
5ϕ	0.05	0.35	0.15	0.40	14.94	20.0	6.85 %
10ϕ	0.06	0.43	0.15	0.40	11.16	15.0	1.26%
20ϕ	0.05	0.43	0.15	0.40	10.14	14.0	8.58%

* ratio between the area limited by the experimental and the numerical curves and the area underneath the experimental curve.

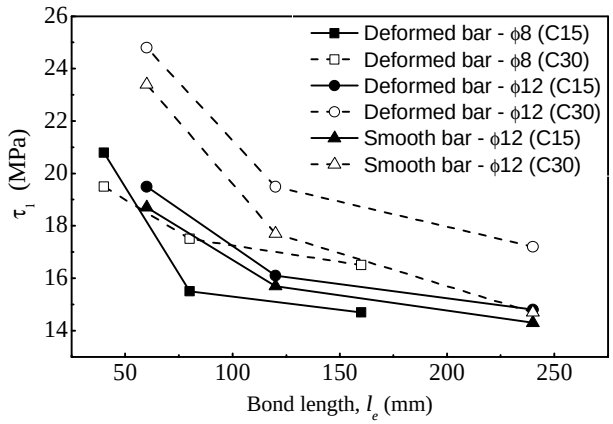

Figure 10. Maximum theoretical bond stress versus embedment length.

4.6 *Slip at maximum bond stress*

The influence of L_e on the slip at the end of the plastic phase, δ_2, is shown in Figure 11, where it is visible that δ_2 increases with the embedment length of GFRP bar. The values of δ_2 in case of specimens with 30 mm concrete cover are higher than those with 15 mm concrete cover thickness.

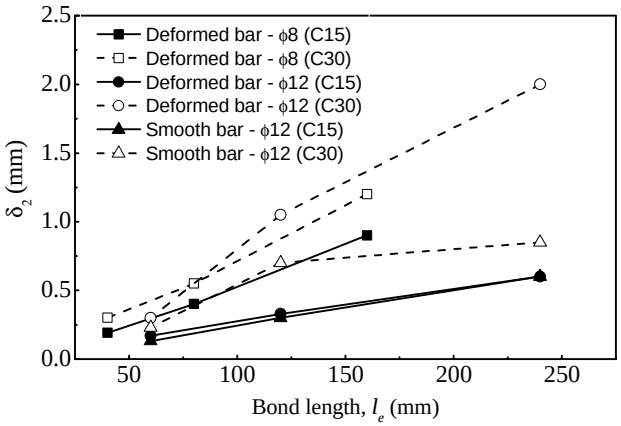

Figure 11. Slip at the maximum bond stress versus the embedment length.

4.7 *Residual bond stress*

Figure 12 compares the ratio between residual bond stress (τ_3) and the maximum bond stress (τ_1) for all the specimens. As shown in this figure, for each type of surface and specific bar diameter, the ratio shows the higher value for specimens with 30 mm concrete cover than those with concrete cover of 15 mm. The higher concrete confinement provided when adopting larger concrete cover can justify this behavior. The ratio ranged 38%-67% for all specimens.

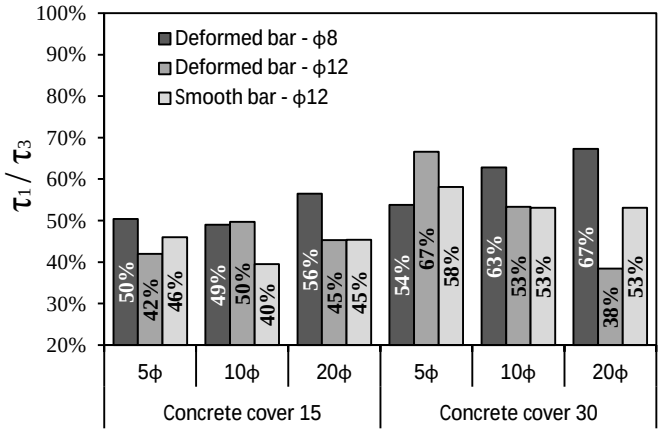

Figure 13. The ratio between residual bond stress and the maximum bond stress.

5 CONCLUDING REMARKS

An analytical model to solve the nonlinear differential equation, which governs the bond between GFRP bar and steel fiber reinforced self compacting concrete (SFRSCC), was presented by adopting a 4-linear bond-slip constitutive law. The good predictive performance was evidenced by simulating the pullout force versus loaded end slip responses registered in experimental tests; however, the accuracy of the model in terms of

estimating the free end slip has decreased with the increase of the bond length of the bar.

- An interface finite element with a non-linear constitutive law was adopted to simulate numerically the bond behavior between GFRP bar and surrounding SFRSCC. The model provided accurate simulation for both deformed and smooth GFRP bars (in case of 5 ϕ and 10ϕ bond length); however, deficient predictions were obtained when simulating the tests with smooth (sand-coated) bar of 20ϕ bond length, since the model was not able of capturing the abrupt load decay registered in these experimental tests.
- Base on the experimental results, the maximum average bond stress ($\bar{t}_m$) decreased when the embedment length of GFRP bar increased. This confirms by means of the maximum analytical bond stress (τ_1) obtained from the bond model.
- A residual bond stress was observed for both GFRP bars utilized in this study. The residual bond stress (τ_3) is influenced with confinement provided by concrete cover thickness.

ACKNOWLEDGMENT

The authors acknowledge support provided by FCT - Fundação para a Ciência e a Tecnologia. The study presented in this paper is a part of the research project titled "DURCOST - Innovation in reinforcing systems for sustainable pre-fabricated structures of higher durability and enhanced structural performance" with reference number of PTDC/ECM/105700/2008. The authors also thank the collaboration of the following companies: Schock for providing the GFRP bars, Casais to manufacture the moulds, Maccaferri for supplying the steel fibers, Secil/Unibetão for providing the Cement, SIKA for providing the superplasticizers; CiviTest for the production of SFRSCC specimens**.**

6 REFERENCES

Achillides, Z. & Pilakoutas, K. 2004. Bond Behavior of Fiber Reinforced Polymer Bars under Direct Pullout Conditions. *Journal of Composites for Construction* 8 (2): 173-181.

Aiello, M. A., Leone, M. Pecce, M. 2007. Bond Performances of FRP Rebars-Reinforced Concrete. Journal of Material in Civil Engineering 19 (3): 205-213.

AL-Mahmoud F., Castel A., Francois R., Tourneur C. 2007. Effect of surface pre-conditioning on bond of carbon fiber reinforced polymer rods to concrete. *Cement & Concrete Composites* 29 (9): 677–689.

Baena M., Torres L., Turon A., Barris C. 2009. Experimental study of bond behavior between concrete and FRP bars using a pull-out test. Composite Part: B 40 (8): 784-797.

Barros, J. A. O., Costa, I. G., Ventura-Gouveia, A. 2011. CFRP flexural and shear strengthening technique for RC beams: experimental and numerical research. *Advances in Structural Engineering Journal* 14 (3): 559-581.

Bianco, V, Barros, J. A. O., Monti, G. 2009. Bond Model of NSM-FRP Strips in the Context of the Strengthening of RC Beams. *Journal of Structural Engineering* 135 (6): 619-631.

Davalos, J. F., Chen Y., Ray, I. 2008. Effect of FRP bar degradation on interface bond with high strength concrete. *Cement & Concrete Composites* 30 (8): 722-730.

Dias, S. J. E.; Barros, J. A. O. 2011. Shear strengthening of RC T-section beams with low concrete using NSM CFRP laminates. *Journal Cement & Concrete Composites* 33 (2): 334-345.

Eligehausen, R., Popov, E. P., and Bertero, V. V. 1983. Local bond stress-slip relationships of deformed bars under generalized excitations. Rep. No. 83/23, *Environmental Engineering Research Council*, University of California, Berkeley, Calif.

Focacci, F., Nanni, A., Fellow, ASCE, Bakis, C. E. 2000. Local bond-slip relationship for FRP reinforcement in concrete. *Journal of Composites for Construction* 4 (1): 24-31.

Hao Q., Wang Y., He Z., Ou J. 2009. Bond strength of glass fiber reinforced polymer ribbed rebars in normal strength concrete. *Construction and Building materials* 23 (2): 865-871.

Lee J. Y., Kim, T. Y., Kim, T. J., Yi, C. K., Park, J. S., You, Y. C., Park, Y. H. 2008. Interfacial bond strength of glass fiber reinforced polymer bars in high-strength concrete. *Composites Part B* 39 (2): 258–270.

Mazaheripour, H., Barros, J., Soltanzadeh, F., Gonçalves, D., Interfacial bond behaviour of GFRP bar in self-compacting fiber reinforced concrete, 8th RILEM international symposium on fibre reinforced concrete: Challenges and Opportunities (BEFIB 2012), Guimarães, Portugal.

Okelo R., A.M.ASCE, Yuan R. L., P. E., M.ASCE. 2005. Bond Strength of Fiber Reinforced Polymer Rebars in Normal Strength Concrete. *Journal of Composites for Construction* 9 (3): 203-213.

Pepe, M. 2011. Experimental and numerical study on bond behaviour of GFRP bars in high-strength fiber-reinforced concrete. M.Sc. Thesis, Dept. of Civil Eng., University of Minho, Portugal (supervisor: Prof. Dr. Joaquim A.O. Barros) - University of Salerno, Italy (supervisor Dr. Enzo Martinelli)

RILEM. Bond test for reinforcement steel 1. Beam test. 1982; TC9-RC.

Robert M., Benmokrane B. 2010. Effect of aging on bond of GFRP bars embedded in concrete. Cement & Concrete Composites 32 (6): 461-467.

Russo, G., Zingone, G., and Romano, F. 1990. Analytical solution for bond-slip of reinforcing bars in R.C. joints. Journal of Structural Engineering 116 (2): 336–355.

Sena-Cruz, J. M. Strengthening of concrete structure with near-surface mounted CFRP laminate strips. *PhD thesis*. Guimaraes, University of Minho, 2004.

Vitor Cunha. Steel Fibre Reinforced Self-Compacting Concrete (from Micro-Mechanics to Composite Behaviour). *PhD thesis*. Guimaraes, University of Minho, 2010.